A Molecular Envelope of the Ligand-Binding Domain of a Glutamate Receptor in the Presence and Absence of Agonist†

Rupert Abele,‡ Dmitri Svergun,§,|| Kari Keinänen,⊥ Michel H. J. Koch,§ and Dean R. Madden*,‡

Ion Channel Structure Research Group, Max Planck Institute for Medical Research, Jahnstrasse 29, 69120 Heidelberg, Germany, European Molecular Biology Laboratory, Hamburg Outstation, EMBL c/o DESY, Notkestrasse 85, 22603 Hamburg, Germany, Institute of Crystallography, Russian Academy of Sciences, Leninsky pr. 59, 117333 Moscow, Russia, and Viikki Biocenter, Department of Biosciences, Division of Biochemistry, P.O.B. 56, FIN-00014 University of Helsinki, Finland

Received December 14, 1998; Revised Manuscript Received March 24, 1999

ABSTRACT: Solution scattering studies were performed on a ligand-binding domain (S1S2) of a glutamate receptor ion channel (GluR) in order to study GluR-binding and signal-transduction mechanisms. The core of the ligand-binding domain is homologous to prokaryotic periplasmic binding proteins (PBP), whose binding mechanism involves a dramatic cleft closure: the "Venus flytrap". Several models of GluR function have proposed that a similar cleft closure is induced by agonist binding. We have directly tested this putative functional homology by measuring the radius of gyration of S1S2 in the presence and absence of saturating concentrations of agonists. In contrast to the PBP, S1S2 shows no reduction in radius of gyration upon agonist binding, excluding a comparably large conformational change. Furthermore, we determined an ab initio molecular envelope for our S1S2 construct, which also contains the peptides that connect the PBP homology core to the three transmembrane domains and to an N-terminal domain. By fitting an atomic model of the ligand-binding domain core to the envelope of our extended construct, we were able to establish the likely position of these connecting peptides. Their positions relative to one another and to the expected sites of an agonist-induced conformational change suggest that ion channel gating and desensitization may involve more subtle and complex mechanisms than have been assumed based on the structural homology to the PBP.

Fast excitatory synaptic transmission in the central nervous system is mediated primarily by glutamate receptor ion channels (*1*−*4*), which are thought to play an important role in learning and memory (*5*) as well as in disease (*6*). The glutamate receptors (GluR)[1] are oligomeric channels formed by subunits 900−1500 amino acids in length. They are classified into pharmacological subfamilies according to their affinity for the agonists α-amino-3-hydroxy-5-methyl-4-isoxazole propionate (AMPA), *N*-methyl-D-aspartate (NMDA), and kainate (*3, 7, 8*). Like many ligand-gated ion channels, the GluR also exhibit desensitization, in which the channel closes despite the continuing presence of certain agonists.

GluR ligand binding is mediated by an extracellular domain with homology to the prokaryotic periplasmic binding proteins (PBP) (*2, 9*−*11*). This domain can be expressed as a soluble protein that reproduces the binding affinity of the solubilized intact receptor, at least for GluR subunits belonging to the AMPA receptor subfamily (*11, 12*). It consists of approximately 150 amino acids prior to the first transmembrane segment (S1) and the approximately 150 amino acid long extracellular loop between the second and third transmembrane segments (S2). Located within the S2 sequence is a 38 amino acid long peptide encoded by alternatively spliced exons ("flip" and "flop"), whose identity influences desensitization kinetics (*13*).

In analogy to the "Venus flytrap" binding mechanism shown for the PBP (*14*−*19*), it has been proposed that the GluR ligand-binding domain is composed of two lobes that close down to sequester ligand in the cleft between them and that the associated conformational change initiates channel gating and/or desensitization (*20*−*22*). Ligand binding is communicated to the transmembrane domains via short peptides that connect them to the central or "core" PBP homology domain (*23*); these peptides do not exhibit PBP homology and therefore have been excluded from modeling studies (*24*). They were also excluded from an S1S2 construct whose crystal structure was recently determined in complex with the nondesensitizing agonist kainate (*25*).

† Financial support was provided in part by EU grants of the Fourth Framework Program in Biotechnology (BIO4-CT96-0589 to D.R.M. and K.K.; BIO4-CT97-2143 to D.S.) and the Academy of Finland (K.K.).

* Correspondence should be addressed to this author at ICSRG, Max Planck Institute for Medical Research, Jahnstrasse 29, 69120 Heidelberg, Germany. Telephone: +49-6221-486150. Fax: +49-6221-486437. E-mail: madden@mpimf-heidelberg.mpg.de.

‡ Max Planck Institute for Medical Research.

§ European Molecular Biology Laboratory.

|| Russian Academy of Sciences.

⊥ University of Helsinki.

[1] Abbreviations: GluR, glutamate receptor(s); PBP, periplasmic binding proteins; R_g, radius of gyration; AMPA, α-amino-3-hydroxy-5-methyl-4-isoxazole propionate; NMDA, *N*-methyl-D-aspartate; SAXS, small-angle X-ray scattering; D_{max}, maximum intraparticle interatomic distance.

10.1021/bi982928y CCC: $18.00
Published on Web 08/05/1999

This structure determination confirmed the similarity of the core of an AMPA receptor ligand-binding domain and the PBP; the closest homology is to the glutamine-binding protein (*25*). Kainate is bound in a cleft between two globular subdomains. In the absence of an apo structure, it is not possible to establish the conformational changes associated with ligand binding; however, the kainate complex appears to have a structure intermediate to the open and closed forms of the glutamine-binding protein. The authors postulate that the desensitizing agonists AMPA and glutamate would allow the cleft to close relative to the kainate structure. This speculation is in line with the earlier proposal that desensitization is triggered by cleft closure (*21*).

To assess the nature of the conformational change induced by agonist binding, we have compared the solution scattering properties of the free and agonist-bound states of a ligand-binding domain of the AMPA receptor subunit GluRD. Unlike published models or atomic structures (*24*, *25*), our construct includes the peptides linking the PBP homology core to the transmembrane domains. We have determined a molecular envelope for this construct in solution, and fit a published model to it; this permitted us to localize the peptides that link the core homology domain to the transmembrane domains.

MATERIALS AND METHODS

Protein Expression and Purification. The S1S2 construct described in Kuusinen et al. (*11*) was overexpressed in *Trichoplusia ni* High Five cells as previously described (*26*). After 66 h of infection, up to 8 L of medium was cleared of cells and viruses by centrifugation and filtering. Cells were removed by centrifugation at 4000*g* for 30 min. The supernatant was cleared of viruses and cell debris by a filter system consisting of a Durapore membrane with pore size of 5 μm (Millipore) and a tangential flow filter (300K TFF-filter, Millipore) with a molecular mass cutoff of 300 kDa. The volume of the filtrate was reduced to 1 L by a 30K TFF-filter (Millipore) with a molecular mass cutoff of 30 kDa. $CaCl_2$ was added to the retentate to a final concentration of 3 mM. The retentate was loaded onto a 25 mL anti-FLAG M1 affinity gel column (Kodak) preequilibrated with washing buffer (10 mM Tris-HCl, pH 7.4, 140 mM NaCl, 3 mM $CaCl_2$). The column was washed with washing buffer until the protein concentration of the wash was less than 10 μg/mL. Bound protein was eluted with 10 mM Tris-HCl, pH 7.4, 140 mM NaCl, 2 mM EDTA. Protein-containing fractions from the FLAG-column were loaded onto an anion exchange column (Poros-20-HQ, Perseptive Biosystems) preequilibrated with 10 mM Tris-HCl, pH 8.0. The bound protein was eluted with a 0−1 M NaCl gradient. The appropriate fractions were pooled. The protein was extensively dialyzed against 50 mM Tris-HCl, pH 7.4, 100 mM NaCl, 0.02% (w/v) NaN_3 and concentrated with a Centricon concentrator with a molecular mass cutoff 10 kDa (Amicon) to 25 mg/mL. The protein concentration was determined by the method of Bradford (*27*).

Equilibrium Dialysis. Equilibrium dialysis half-chambers with a volume of 60 μL each were separated by a dialysis membrane with a cutoff pore size of 6−8 kDa (Spectrapor). One half-chamber was filled with 10 mM NaP_i, pH 7.3, and a mixture of 1.5 μM [^{3}H]-L-glutamate (NEN DuPont) and 13.5 μM cold L-glutamate. The other half-chamber contained the same solution supplemented with 1 μM S1S2. The chambers were allowed to equilibrate for 15 h at 4 °C. Then 10 μL from each half chamber was mixed with 5 mL of scintillation fluid (Packard Instruments) and the radioactivity determined with a Beckman scintillation counter LS 6500. For each L-glutamate concentration, triplicates were prepared. The equilibrium constant K_d of S1S2 for L-glutamate as determined by equilibrium dialysis is 1 μM (*26*).

Fluorescence Titration. The fluorescence titrations were measured with an SLM 8000 spectrofluorometer. The excitation band-pass was 4 nm, and the sample cell was maintained at 5 °C with a circulating water bath. All measurements were determined as the ratio between the fluorescence change of the sample and a reference cuvette filled with rhodamine to reduce the noise due to intensity fluctuations of the Xenon lamp. The excitation wavelength was 280 nm for all measurements, and the fluorescence change of the titration measurements was monitored at 336 nm. Aliquots of 10 μL of concentrated ligand were added to a quartz cuvette containing 3 mL of protein (0.08−0.13 μM) in 10 mM NaP_i, pH 7.3, under continuous mixing with a magnetic stirrer. For each glutamate concentration, 20−25 data points were averaged (each data point was a mean of 3 s). The change of fluorescence was corrected for the dilution of the sample with glutamate. The results were fitted using the equation:

$$F_i = F_0 + \frac{(E_0 + L + K_d) - \sqrt{(E_0 + L + K_d)^2 - 4E_0L}}{2E_0/\Delta F_{max}}$$

where F_i is the fluorescence observed after the ith addition of glutamate, F_0 the fluorescence of the free protein, E_0 the protein concentration, L the added ligand concentration, K_d the dissociation constant, and ΔF_{max} the maximum fluorescence change in going from unbound to completely bound protein.

Small-Angle X-ray Scattering Measurements and Data Analysis. Small-angle X-ray scattering (SAXS) measurements were performed in the concentration range from 2.5 to 20 mg/mL S1S2 without or with 0.5 mM glutamate on the double-focusing monochromator-mirror camera X33 of the EMBL (*28*) on the storage ring DORIS of the Deutsches Elektronen Synchrotron at Hamburg at a wavelength λ = 0.15 nm using a quadrant detector (*29*). Two sample−detector distances (3.5 and 1.2 m) covered the ranges of momentum transfer $0.18 < s < 2.0$ nm^{-1} (setting 1) and $0.40 < s < 4.5$ nm^{-1} (setting 2), respectively ($s = 4\pi \sin \theta/\lambda$, where 2θ is the scattering angle). The scattering curves of the protein solutions and the corresponding solvents were collected in 15 one-minute frames to monitor radiation damage and beam stability. The primary data analysis, buffer subtraction, and normalization were done using the program SAPOKO (D.S. and M.H.J.K., unpublished). The maximum diameter of the particle was estimated using the orthogonal expansion method (*30*). Radii of gyration and the distance distributions were computed using the indirect transform method based on the regularization technique as implemented in the program GNOM (*31*, *32*).

The molecular mass (M_r) of S1S2 was calculated by the equation:

$$M_r(\text{S1S2}) = \frac{M_r(\text{BSA}) I_{\text{S1S2}}(0) c_{\text{BSA}}}{I_{\text{BSA}}(0) c_{\text{S1S2}}}$$

where $I(0)$ is the forward scattering and c is the protein concentration. Bovine serum albumin was used as standard with a known molecular mass of 66 kDa.

Shape determination of the agonist-free particle was performed using multipole expansion methods. The experimental data from setting 1 were fitted ab initio by the scattering from an envelope function starting from a spherical initial approximation (*33*). The envelope was represented with spherical harmonics using 10 free parameters, which is justified given the information content in the data used (7 Shannon channels) (*34*).

Calculation of Radius of Gyration, Scattering Curve, Envelope Functions, and Intraparticle Distances from Atomic Coordinates. The coordinate sets for the holo and apo forms of the model of the ligand-binding domain of GluRA used were obtained from http://web.vet.cornell.edu/public/pharmacology/pdbfiles.html (*24*). Atomic coordinates of the GluRB ligand-binding core domain were obtained from the Protein Data Bank (1GR2) (*25*). Radii of gyration (R_g), maximum intraparticle distances (D_{max}), envelope functions, and scattering curves were calculated from these atomic coordinates using the program CRYSOL taking into account the influence of the hydration shell (*35*).

The position of the GluRA core homology model was found by rotating its envelope function to minimize the discrepancy with the ab initio low-resolution envelope, using an automated procedure. The models were displayed on a SUN Workstation using the program ASSA (*36*).

RESULTS

Radius of Gyration. To assess the conformational changes associated with ligand binding in GluR, SAXS measurements were performed on S1S2. The dependence of R_g on protein concentration is consistent with weak interparticle interactions (Figure 1), and is comparable to that seen for other soluble proteins. However, contrary to the Venus flytrap model, the R_g of S1S2 in the presence of saturating concentrations of the agonist glutamate is *greater* than or equal to the R_g in the absence of agonist at every protein concentration tested and at the values extrapolated to zero protein concentration (R_g = 3.4 nm), within experimental error (Figure 1). Similar observations were made with saturating concentrations of the agonist AMPA, both with and without potassium thiocyanate. Similarly, there is no significant change in the distance distribution function $P(r)$ or in the maximum intraparticle interatomic distance, D_{max} (11 nm), in the presence or absence of glutamate (Figure 2); if anything, agonist-bound S1S2 is slightly less compact than empty S1S2.

Following the experiments, ligand-free protein was recovered from the cuvette and tested for activity, to assess the possibility that radiation damage to S1S2 prevented ligand binding. In equilibrium dialysis experiments, S1S2 exhibited more than 80% specific radioligand binding activity. Moreover, the glutamate affinity determined by fluorescence titration was the same (K_d = 0.5−0.6 μM) as the affinity of untreated S1S2 (R.A. et al., unpublished data). In addition,

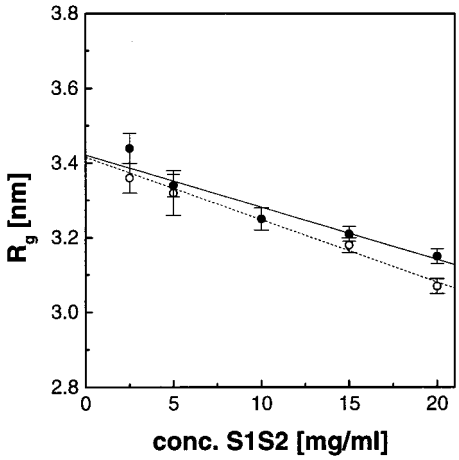

FIGURE 1: Protein concentration dependence of the measured radii of gyration. The radii of gyration are plotted as a function of protein concentration, together with a linear least-squares fit, both in the presence (filled circles, continuous line) and in the absence (open circles, dashed line) of 0.5 mM glutamate. The radius of gyration for zero protein concentration was calculated by extrapolating the straight-line variance-weighted least-squares fits to zero.

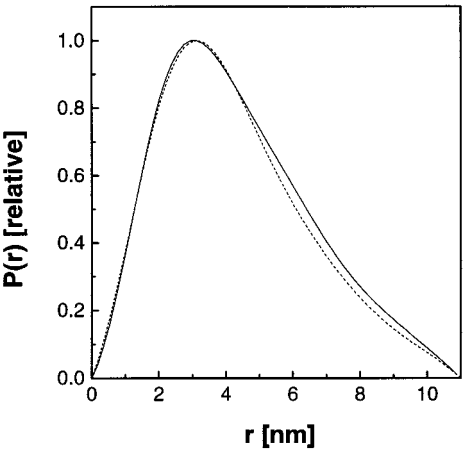

FIGURE 2: Distance distribution plot for S1S2 at 2.5 mg/mL protein concentration in the presence (continuous line) and absence (dashed line) of 0.5 mM glutamate.

no change in the solution scattering was observed over the 15 min time-course of the measurements.

Particle Elongation. A second striking feature is observed in the small-angle scattering data. Both the radius of gyration (ca. 3.4 nm) and the longest intraparticle distance detected (ca. 11.0 nm) are much larger than expected (Figure 2). The X-ray crystallographic structure of a ligand-binding domain core of GluRB in complex with kainate has an R_g = 2.1 nm and a D_{max} = 6.4 nm (*25*). Models of the PBP homology core of the AMPA receptor subunit GluRA have R_g = 2.3 nm and D_{max} = 7.8 nm in the apo form and R_g = 2.2 nm and D_{max} = 7.5 nm in the holo form (*24*). As shown in Table 1, all three models have a molecular mass substantially smaller than that of S1S2. However, even the similar-sized maltose-binding protein (M_r = 41 kDa) exhibits an experimental R_g of less than 2.3 nm and a D_{max} of less than 8.0 nm, after correction for protein concentration effects (*19*). This indicates either that S1S2 in solution is much larger than assumed (e.g., due to oligomerization or aggregation) or that it is very elongated.

The possibility of oligomerization or aggregation of S1S2 was ruled out by a number of methods. First of all, the

Table 1: RMS Difference of Calculated vs Observed Solution Scattering for Models of the GluR Ligand-Binding Core Domain[a]

		rms ($I_{obs} - I_{calc}$)		
	M_r (kDa)	$d >$ 1.57 nm	$d >$ 3.14 nm	3.14 $> d >$ 1.57 nm
X-ray structure	26.8	4.6	5.5	0.87
closed model	29.4	4.0	4.5	0.97
open model[b]	29.2	3.1	3.5	0.95
S1S2	42.5	−	1.0	−

[a] Scattering curves were calculated for three models: the X-ray structure of the kainate-bound GluRB core domain (*25*) and theoretical models of the open and closed states of the GluRA domain defined by homology modeling with LAOBP (*24*). Fits and rms differences were calculated over three resolution ranges. The rms difference of the ab initio molecular envelope is shown in the row "S1S2" ($d >$ 3.14 nm only). [b] This structure was superimposed on the molecular envelope, as shown in Figure 5.

molecular mass of S1S2 was calculated from the ratio of forward scattering $I(0)$ to protein concentration, using bovine serum albumin as a standard. The resulting value of 45 kDa compares well with the expected monomer value of ca. 42 kDa including glycosylation. Furthermore, the dependence of R_g on protein concentration between 2.5 and 20 mg/mL protein (Figure 1) indicates no change in the size of the particles beyond the apparent decrease due to weak interparticle interference effects. Thus, there is no reversible association of the monomers to form oligomers within this concentration range (60−480 μM). Finally, the volume of an ab initio molecular envelope calculated from the solution scattering data corresponds to that expected for a 42 kDa monomer (see below).

Comparison with Atomic Models. The solution scattering curves of three atomic models for GluR ligand-binding domains were computed and compared to the observed scattering. The atomic models used were the crystal structure of the complex of kainate with a ligand-binding domain core of GluRB (*25*) and theoretical models of the open (apo) and closed (holo) forms of the GluRA ligand-binding domain core (*24*). These molecules all have a substantially smaller molecular mass than S1S2 (Table 1 and Figure 3) and are all much more compact, with R_g less than 2.3 nm. Considering all data, the theoretical model of an open structure gives the best fit to the observed scattering data, and the X-ray structure, the worst fit (Table 1). The relatively poor match of the X-ray structure is partly due to the fact that it is even smaller than the theoretical models (27 kDa vs 29 kDa): truncating the theoretical models to include only those residues present in all three structures yields rms scattering differences for the open and closed GluRA models of 3.4 and 4.3, respectively, the latter comparable to the value obtained for the X-ray model. Even when thus truncated, however, the open model clearly provides the best fit to the experimental data. The superiority of the open model is determined by its better fit to the low-resolution data ($d >$ 3.14 nm), where the quaternary structure of the particle dominates (Table 1). At relatively high resolution (3.14 nm $> d >$ 1.57 nm), where packing of secondary structure elements dominates, the crystallographic structure provides the best fit. A superposition of the observed scattering curve with that calculated for the open GluRA model is shown in Figure 4.

Molecular Envelope. Using the multipole expansion method (*31*), an ab initio molecular envelope was determined for the agonist-free protein at a resolution of about 3.3 nm. As expected based on the large R_g and D_{max} values for S1S2, the restored envelope of the ligand-binding domain (Figure 5) is a highly elongated particle (axial ratio 3:1), whereas the PBP themselves are somewhat less elongated (axial ratio 2:1). The volume of the molecular envelope is 84 nm^3. Assuming a specific volume of 1.8 nm^3 kDa^{-1}, as observed for other proteins using this technique (*37*), this corresponds to a molecular mass of ca. 47 kDa, confirming that the protein is indeed monomeric under the experimental conditions.

Given that it best fit the observed scattering in the appropriate resolution range, the theoretical model of the open form of the ligand-binding domain core of GluRA (*24*) was superimposed on the envelope (Figure 5). As both the envelope and the model exhibit two distinct unequal subdomains (lobes), they could be positioned unambiguously with respect to each other. The fits to the experimental data provided by the restored envelope and by the model (Figure 4) indicate that the envelope yields much better agreement than the model at low angles (Table 1). The scattering in this range reflects the quaternary structure of the particle, and it was thus used for the shape determination. At higher angles, corresponding to ca. 1.57−3.14 nm resolution, scattering from the internal particle structure dominates, particularly from the packing of secondary structure elements. Since the ab initio envelope has no internal structure, the atomic models all yield a better fit in this region. Despite their incompleteness, their arrangement of secondary structure elements is broadly correct and therefore a much better approximation to the internal structure of the scattering particle than a homogeneous envelope. It can be concluded that the various model coordinates provide a fair representation of the secondary structure of S1S2 [as confirmed by the crystallographic structure of a related domain (*25*)], but fail to match its quaternary structure due to peptide sequences absent from the model.

S1S2 includes peptide sequences that connect the core PBP homology domain to the N-terminal X-domain and to the three transmembrane domains [traditionally referred to as membrane-associated domains M1, M3, and M4; M2 forms a reentrant pore loop (*8*)]; it also contains two glycosylation sites near the N-terminus (Figure 3). These moieties (boldface sequences and asterisks in Figure 3) are absent from the GluRA model (*24*) and are also absent from the recently determined GluRB crystal structure (*25*). In addition to these native sequences, linker and purification peptides are included in the construct studied here (italic sequences in Figure 3). Since the volume of the molecular envelope corresponds to the molecular mass of S1S2 and since the atomic model fits completely within the envelope (Figure 5), the unoccupied volume must be consistent with the molecular mass present in S1S2 but missing from the model. Positioning the additional moieties in the empty space at the ends of the particle is thus sufficient both to fill out the envelope and to account for its observed elongation relative to the structure of the core domain.

As indicated in Figure 3, these additional moieties can be grouped into three peptides. Based on the location of the N- and C-termini of the S1 and S2 peptides in the GluRA PBP

```
                Peptide I                                      Peptide II                                                Peptide III
S1S2  : DYKDDDDKISRPTLGNDTAA IENR..(S1).. KKP QKSKPGVFSFLDPLAYE STEGEVNAEEEGF ERMVSPIE SAE..(S2).. CGPK DSGSKDKTSALSLSN ELEQKLISEEDLN
GluRD :             TLGNDTAA IENR..(S1).. KKP QKSKPGVFSFLDPLAYE (M1).....(M3) ERMVSPIE SAE..(S2).. CGPK DSGSKDKTSALSLSN (M4)
Model :                      VQNR..(S1).. KKP                                      SAE..(S2).. CGTG
X-ray :                         K..(S1).. K                                      E SAE..(S2).. C
         --FLAG--  |                                    |---LINKER----|                                       |----C-MYC----
                  383  *      *                        525           628                                     792
```

FIGURE 3: Sequence comparison of S1S2 to GluRD, the PBP homology core model of GluRA ("Model") (*24*), and the crystal structure of the PBP homology core of GluRB ("X-ray") (*25*). The GluRA model was used in fitting the experimental molecular envelope shown in Figure 5. Peptide sequences present in S1S2 but absent from the GluRA model are shown in boldface (native GluRD sequences) or italics (non-native fusion protein sequences). Connections to other domains in GluRD are indicated in parentheses within the GluRD sequence. The core S1 and S2 sequences have been omitted and are indicated by parentheses in all sequences. Residues present in the GluRB construct but not located in the X-ray structure have been omitted from the "X-ray" sequence. The FLAG and c-myc epitopes and the linker peptide are indicated below the S1S2 sequence, as are the locations of N-linked glycosylation sites (asterisks) and sequence numbers corresponding to the mature sequence of GluRD. The three peptides referred to in the text and in Table 2 are shown as shaded boxes within the S1S2 sequence.

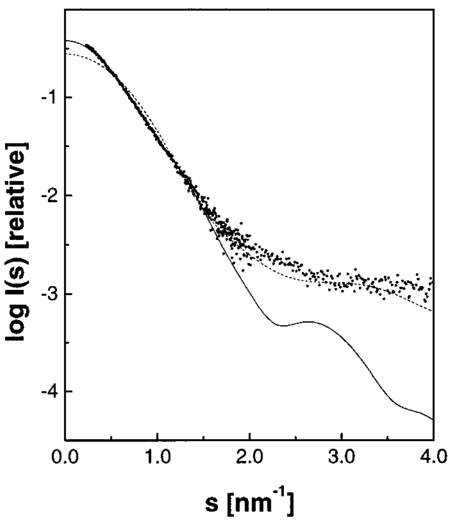

FIGURE 4: Composite scattering curve from S1S2 obtained by merging the experimental data (dots) from setting 1 ($0.18 \le s \le 2.0$ nm^{-1}) and setting 2 ($0.40 \le s \le 4.5$ nm^{-1}) shown together with the theoretical scattering calculated from the restored envelope (solid line) and from the GluRA core homology model (dashed line).

homology core model and the fit of that model into the envelope, we have located the approximate positions of these additional sequences within the molecular envelope and relative to the homology core (Figure 5). The molecular masses of the peptides and the proportions of each derived from native and non-native moieties are shown in Table 2.

Peptide I includes the connection from S1S2 to the N-terminal X-domain of GluR. Based on the position of the N-terminus of S1 (arrows "1" in Figure 5), peptide I must be located near the top end of the particle as shown in Figure 5A,B (purple spheres).

Peptide II contains the amino acids linking the ligand-binding core domain to transmembrane domains M1 and M3; given the position of the S1 C-terminus and S2 N-terminus (arrows "2" in Figure 5), peptide II must be located at the opposite end of the particle from peptide I (Figure 5, green spheres). Peptides I and II are thus oriented toward the ends of the particle, away from each other and away from the hinge/cleft region at the center of the particle.

Peptide III contains part of the flip/flop alternative splicing sequence and connects the ligand-binding core domain to transmembrane domain M4. Its attachment point is located near the center of the atomic model (arrows "3" in Figure 5) and, in order for the transmembrane domains of one GluR subunit to cluster, it would have to be positioned along the

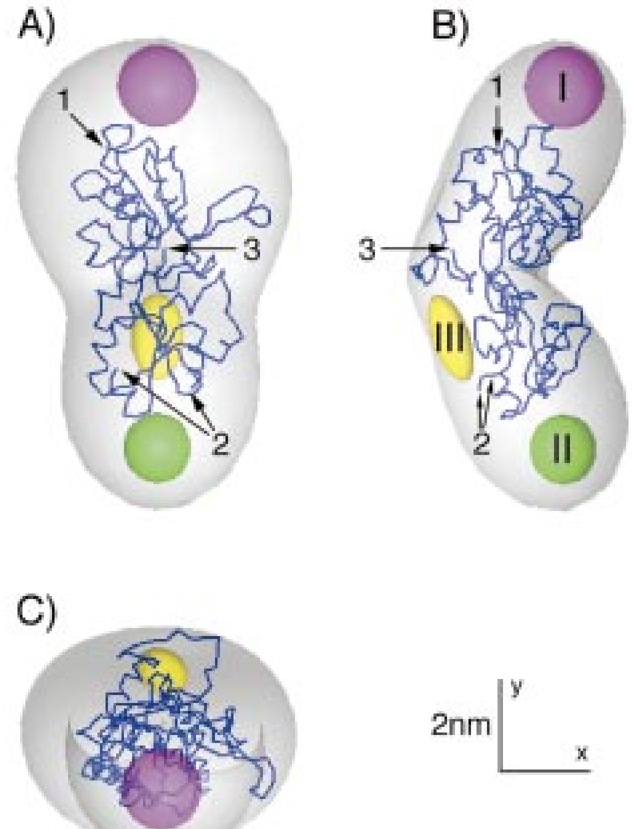

FIGURE 5: (A) Ab initio molecular envelope of the agonist-free form of the S1S2 particle (semi-transparent solid) superimposed on the GluRA open model (blue C_α trace). The low-resolution envelope includes a 0.3 nm wide interface layer of gradual density decrease from protein to the bulk solvent, emulating the hydration effects. Views shown in (B) and (C) are obtained by a right-handed 90° rotation of the envelope shown in (A) about the *y* and *x* axes, respectively. The peptides I, II, and III are represented by the purple, green, and yellow solids, respectively, with volumes proportional to the total molecular masses in Table 2. Peptide II is omitted from (C); it is completely obscured by peptide I in this orientation. (A, B) The connections of peptides I, II, and III to the model N- and C-termini are indicated by arrows labeled 1, 2, and 3, respectively.

back of the particle (Figure 5, yellow ellipsoids), pointing from the hinge toward peptide II. The connections to the three transmembrane domains would emerge from the bottom half of the particle in the orientation shown in Figure 5.

Although the open model was chosen for superposition on the molecular envelope, it should be emphasized that both the closed model and the X-ray structure also can be accommodated satisfactorily in the equivalent orientation

Table 2: Distribution of Molecular Mass in S1S2[a]

	M_r (kDa)		
	total	native	non-native
peptide I	ca. 6.0[b]	ca. 4.7[b]	1.3
peptide II	4.2	2.9	1.3
peptide III	3.1	1.5	1.6
peptides I−III	ca. 13.3[b]	ca. 9.1[b]	4.2
GluRA model	29.2	29.2	0.0
total	42.5[b]	38.3[b]	4.2

[a] Molecular masses are shown for GluRD peptides not included in the GluRA model and connecting the ligand-binding domain core to the X-domain and transmembrane domains ("native") and for fusion sequences ("non-native"), clustered into peptides I−III as shown in Figure 3. [b] Value includes a total of ca. 4 kDa for N-linked glycosylation at the two sites in and adjacent to peptide I (asterisks in Figure 3).

within the envelope. A least-squares superposition of the X-ray structure and the open model is shown in Figure 6. Because of its smaller molecular mass and slightly more compact shape, the X-ray structure more completely fills the envelope at its "waist", and leaves slightly larger spaces at the two ends. Regardless of the model chosen, the location of unfilled volumes within the envelope and the points of attachment for peptides I−III are conserved.

DISCUSSION

Solution scattering experiments have consistently revealed a reduction in the radius of gyration of the PBP upon ligand binding of approximately 0.1 nm and a reduction of the maximum intraparticle distance of 0.5−1.0 nm. Crystal structures have been determined of various PBP, revealing a bilobate structure with a prominent cleft: both ligand-free structures with an "open" cleft and ligand-bound structures with a "closed" cleft have been observed (*14*−*19*). Taken together, these data provide strong evidence for the so-called "Venus flytrap" binding mechanism for the PBP (*15*), in which the equilibrium between open and closed forms favors the open form in the absence of ligand and the closed form in its presence. The ligand is trapped within the closed cleft. A homologous bilobate structure with agonist bound in the cleft has been confirmed by the crystallographic structure of the ligand-binding core domain of GluRB in complex with kainate (*25*). However, in contrast to expectations based on the PBP homology, S1S2 does not show a reduction of R_g or D_{max} upon ligand binding. Also, the distance distribution functions in the presence and absence of agonist agree closely. This appears to exclude a large structural rearrangement of S1S2, similar to that seen in the PBP, following agonist binding.

We can exclude the possibility that these observations are due to the fact that the ligand-free protein was not competent to bind ligand. The protein exhibited normal affinity and specific binding activity following SAXS measurements, using both (rapid) fluorescence and (slow) equilibrium dialysis techniques. It can also be excluded that endogenous ligand copurified with the protein, as has been observed for certain PBP (*38*). Purified S1S2 has been shown to have a single class of binding sites and to have 100% of the binding sites expected based on 1:1 ligand-binding stoichiometry (*26*). Also, agonist binding is a rapid, second-order process (*39*). Both of these observations are inconsistent with the properties of PBP whose binding sites were constitutively occupied (*38*).

The lack of observable cleft closure is also unlikely to be due to the fact that the ligand-binding domain favors the closed conformation even in the absence of ligand. This has been observed for certain PBP. The crystal structure of an unliganded, closed form of the glucose/galactose-binding protein has been determined, and a closed conformation in the absence of ligand has been proposed for the C4-dicarboxylate-binding protein from *R. capsulatus* on the basis of ligand-binding kinetics (decrease of k' with increasing ligand concentration) (*40, 41*). The kinetics of agonist binding to purified S1S2 have been determined and show instead an increase of k' with increasing agonist concentration (*39*), ruling out the hypothesis that there is a substantial population of ligand-free S1S2 molecules in a closed conformation, unless the open−closed transition is very rapid compared to ligand binding (*42*). Indeed, the values of k_{on} and k_{off} calculated assuming a one-step binding mechanism are similar to those obtained for PBP thought to exhibit Venus flytrap behavior (*43, 44*). The large axial ratio of the particle, the shape of the molecular envelope (Figure 5), and the fact that the observed low-resolution scattering is best matched by that of an open model of the GluRA domain (Table 1) are also inconsistent with the hypothesis that S1S2 is in a conformation comparable to the "closed" form of the PBP.

Data from X-ray crystallographic (*25*) and kinetic (*39*) studies support the similarity in both structure and binding mechanism of the GluR ligand-binding domains to the PBP. The crystal structure also shows that the kainate complex adopts a conformation intermediate between the open and closed forms of the glutamine-binding protein. Thus, the most straightforward interpretation of our results is that the "flytrap" closes, but does so much more subtly in S1S2 than in the PBP. Small rearrangements cannot be identified by small-angle scattering techniques. For comparison, Lac repressor's binding to operator DNA is controlled by relatively small allosteric effects: a 10° rotation between two subdomains is observed (*45*). In the case of both LacI and GluR, conformational changes may be limited by the requirement for oligomerization (*46*).

The apparent absence of a dramatic cleft closure upon agonist binding may also reflect structural restraints imposed by a disulfide bridge formed within the GluR ligand-binding domains. The cysteine residues involved are conserved throughout all GluR subunits. This disulfide does not exist in the PBP, and it connects two loops that move apart upon PBP cleft closure; it has therefore been proposed that it reduces ligand affinity by introducing strain into the bound conformation (*24*). Consistent with this hypothesis, removal of the putative disulfide bridge by reducing agents or site-directed mutagenesis results in a slight increase in agonist affinity (*47, 48*). The existence of the disulfide bond has now been confirmed biochemically in S1S2, even though the agonist affinity of AMPA receptors is not modulated by reducing agents. Furthermore, elimination of this disulfide bond by site-directed mutagenesis has the expected effect of increasing S1S2 affinity for agonists 2−3-fold (*26*). The small size of the effect is also consistent with a relatively modest overall conformational change upon ligand binding.

The fact that S1S2 reproduces the pharmacology of intact detergent-solubilized GluR (*11*) suggests that the results

FIGURE 6: Stereo superposition of ligand-binding core domain structures determined by X-ray crystallography (*25*) for GluRB (thin line) and by homology modeling (*24*) for GluRA (thick line). The structures were superimposed by a least-squares fit of corresponding Cα positions (*54*). The two structures occupy comparable volumes. The N- and C-termini of the S1 and S2 fragments are marked by gray (GluRB) and black (GluRA) spheres. Only residues common to both models (Figure 3) are shown, so that the termini are slightly displaced from those shown in Figure 5. A gap is present in the GluRB crystal structure (upper right). The orientation of the molecules corresponds closely to the view in Figure 5A.

presented here apply to the intact receptor as well. Indeed, if the experimentally observed lack of a large cleft closure in S1S2 were an artifact of the construct, one should detect a dramatic loss of affinity for agonist: when the leucine-isoleucine-valine-binding protein is trapped in the open conformation by crystal lattice contacts, its affinity for ligands is weakened by several orders of magnitude (*49*). The physiological relevance of the S1S2 construct is further supported by the observation that deletion of a conserved disulfide bridge has the same effect on ligand affinity as cysteine mutagenesis or redox modulation on intact GluR (*26*).

It is not completely clear whether the conformation adopted by the soluble protein corresponds to the resting or the desensitized state of the intact receptor in the membrane. However, the affinity for glutamate of both S1S2 and intact, solubilized GluR (*11, 39*) is significantly higher than the EC_{50} values measured for activation of recombinant GluR ion channels in situ and is more in line with K_I values (*8*), suggesting that the conformations detected are similar to that of the high-affinity desensitized state of the native channel. Since the phenomena of gating and desensitization are only functionally defined within the context of an intact channel, it is fundamentally difficult to assess the status of a soluble construct. However, the characteristic higher ligand affinity of the desensitized state presumably reflects a particular coupling of the binding site to the rest of the protein and/or a particular conformation of the binding site itself. One approach would therefore be to compare the effects of a panel of site-directed mutations (*50*) on the pharmacologies of both the ligand-binding domain and intact GluR in the membrane. If the affinity changes induced in the soluble domain broadly match the effects on either EC_{50} or K_I of the complete receptor, then it is probable that the domain's binding site is in a conformation approximating that of the resting or desensitized state, respectively.

The crystal structure of an S1S2 core/kainate complex for GluRB led to the model-building prediction that the desensitizing agonists AMPA and glutamate would permit cleft closure relative to the nondesensitizing kainate complex (*25*). This proposal is in line with a model in which channel desensitization correlates with closure of the Venus flytrap (*21*). Our results are not consistent with these predictions; neither the distance distribution functions nor the molecular envelope supports the hypothesis that desensitization involves a "closed" state of the ligand-binding domain.

The scattering curve calculated from the crystallographic structure of the S1S2 core/kainate complex matches the observed scattering data more poorly than either the open or the closed models based on LAOBP homology. In part this is due to the omission of more residues from the crystallographic structure. However, even following truncation to an equivalent subset of residues, the open LAOBP-based model provides the best overall match. This is due to differences at the level of quaternary structure, suggesting that in solution our extended S1S2 complex is most similar to an open PBP, both in the presence and in the absence of the desensitizing agonist glutamate. These quaternary structure differences may reflect conformational changes due to the presence of the nondesensitizing agonist kainate in the crystallized complex. It is also worth noting that the GluRB core domain constructs generally exhibited relatively high thermodynamic instability (*51*), compared to S1S2, which shows stoichiometric binding activity following incubation at 27 °C over the course of days during insect cell expression (*26*).

S1S2 is substantially more elongated than its PBP homology core alone. Its molecular envelope reveals two subdomains, separated by a bend at the "waist" of the molecule. As a result, it is possible to orient the atomic model of the PBP homology core of GluRA (29 kDa) (*24*) within the envelope (Figure 5), and thus to determine the likely placement of the additional peptides included in S1S2

(Figures 3 and 5). These three peptides contain native sequences implicated in desensitization (*13*, *52*, *53*), and at least two are likely to mediate channel gating due to their position between the ligand-binding and membrane-spanning domains. Specifically, amino acids N-terminal to S1 (peptide I) and amino acids linking S1 and M1 (peptide II) modulate desensitization in NMDA receptors (*52*, *53*). Peptide III contains part of the flip/flop alternative splicing sequence that modulates desensitization phenomena in AMPA GluR (*13*). Peptides II and III contain the sequences linking S1S2 to the transmembrane domains M1, M3, and M4.

Based on the positions of the S1 and S2 N- and C-termini in the PBP core homology domain, all three peptides could have been clustered around the hinge region, poised to sense a cleft closure directly. This would have produced a relatively compact particle, thickened at the waist. Unexpectedly, two of the peptides (I and II) are instead oriented out from the ends of the particle, distant from the putative binding cleft and the hinge, in a position where even the PBP do not alter their conformations upon ligand binding. Only peptide III originates close to the hinge and ligand-binding cleft, and would therefore be likely to sense directly any conformational change at those positions. The overall arrangement yields a long, narrow structure, whose elongation may reflect the structural requirements of close packing of subunits within the oligomeric channel.

While it is possible that Peptides I−III do not assume the same positions in S1S2 as in the intact molecule, the pharmacological similarities between S1S2 and intact GluRD (*11*) indicate that the soluble domain preserves most important features of the ligand-binding process, as discussed above. In addition, at least the N-termini of S1 and S2 and the C-terminus of S1 are relatively well-constrained by the packing of secondary structure elements within the protein, so that the starting and/or ending positions of the peptides are well-localized. Finally, within peptides I−III, native sequences and carbohydrate moieties contribute more than two-thirds of the additional molecular mass ($M_r \approx 9$ kDa vs $M_r \approx 4$ kDa for non-native sequences; Table 2).

As discussed above, the magnitude of any cleft closure upon ligand binding appears to be small. Taken together with the apparent position of peptides I−III, this suggests that the mechanism by which ligand binding is converted to channel opening and then to desensitization is more subtle than would be expected based on the Venus flytrap model.

This work represents the first structural comparison of the agonist-free and agonist-bound states of any GluR or domain thereof. Although the studies need to be extended to other functional states, they strongly suggest that the Venus flytrap cleft closure model must be modified to correctly describe GluR agonist binding. Furthermore, they indicate that S1S2 is much more elongated than the homologous PBP, presumably due to the distal position of peptides connecting the domain to other parts of the protein. These peptides, implicated in gating and/or desensitization phenomena, are thus distant from the ligand-binding site, raising new questions of the structural mechanism by which agonist binding and ion channel gating are coupled.

ACKNOWLEDGMENT

We thank U. Reygers for technical assistance. This work was supported in part by the Departments of Biophysics (K. Holmes) and Cell Physiology (B. Sakmann) at the Max Planck Institute for Medical Research. We thank an anonymous reviewer for pointing out the comparison to LacI. Access to the Supercomputing Resources for Molecular Biology (to R.A., D.R.M.) was provided by EU Human Capital and Mobility Contract ERBCHGECT 940062 to the European Molecular Biology Laboratory.

REFERENCES

1. Keinänen, K., Wisden, W., Sommer, B., Werner, P., Herb, A., Verdoorn, T. A., Sakmann, B., and Seeburg, P. H. (1990) *Science 249*, 556−560.
2. Nakanishi, N., Schneider, N. A., and Axel, R. (1990) *Neuron 5*, 569−581.
3. Nakanishi, S. (1992) *Science 258*, 597−603.
4. Sommer, B., and Seeburg, P. H. (1992) *Trends Neurosci. 13*, 291−296.
5. Brennan, P. A. (1994) *Neuroscience 60*, 691−708.
6. Choi, D. W. (1988) *Neuron 1*, 623−634.
7. Wisden, W., and Seeburg, P. H. (1993) *Curr. Opin. Neurobiol. 3*, 291−298.
8. Hollmann, M., and Heinemann, S. (1994) *Annu. Rev. Neurosci. 17*, 31−108.
9. O'Hara, P., Sheppard, P. O., Thogersen, H., Venezia, D., Haldeman, B. A., McGrane, V., Houamed, K. M., Thomsen, C., Gilbert, T. L., and Mulvihill, E. R. (1993) *Neuron 11*, 41−52.
10. Stern-Bach, Y., Bettler, B., Hartley, M., Sheppard, P. O., O'Hara, P., and Heinemann, S. F. (1994) *Neuron 13*, 1345−1357.
11. Kuusinen, A., Arvola, M., and Keinänen, K. (1995) *EMBO J. 14*, 6327−6332.
12. Chen, G. Q., and Gouaux, E. (1997) *Proc. Natl. Acad. Sci. U.S.A. 94*, 13431−13436.
13. Sommer, B., Keinänen, K., Verdoorn, T. A., Wisden, W., Burnashev, N., Herb, A., Köhler, M., Takagi, T., Sakmann, B., and Seeburg, P. H. (1990) *Science 249*, 1580−1585.
14. Newcomer, M. E., Lewis, B. A., and Quiocho, F. A. (1981) *J. Biol. Chem. 256*, 13218−13222.
15. Mao, B., Pear, M. R., McCammon, J. A., and Quiocho, F. A. (1982) *J. Biol. Chem. 257*, 1131−1133.
16. Quiocho, F. A. (1991) *Curr. Opin. Struct. Biol. 1*, 922−933.
17. Olah, G. A., Trakhanov, S., Trewhella, J., and Quiocho, F. A. (1993) *J. Biol. Chem. 268*, 16241−16247.
18. Oh, B.-H., Pandit, J., Kang, C.-H., Nikaido, K., Gocken, S., Ames, F. L. G., and Kim, S.-H. (1993) *J. Biol. Chem. 268*, 11348−11355.
19. Shilton, B. H., Flocco, M. M., Nilsson, M., and Mowbray, S. L. (1996) *J. Mol. Biol. 264*, 350−363.
20. Wo, Z. G., and Oswald, R. E. (1995) *Trends Neurosci. 18*, 161−168.
21. Mano, I., Lamed, Y., and Teichberg, V. I. (1996) *J. Biol. Chem. 271*, 15299−15302.
22. Laube, B., Hirai, H., Sturgess, M., Betz, H., and Kuhse, J. (1997) *Neuron 18*, 493−503.
23. O'Hara, P. J., Sheppard, P. O., Thogersen, H., Benezia, D., Haldeman, B. A., McGrane, B., Houamed, K. M., Thomsen, C., Gilbert, T. L., and Mulvihill, E. R. (1993) *Neuron 11*, 41−52.
24. Sutcliffe, M. J., Wo, Z. G., and Oswald, R. E. (1996) *Biophys. J. 70*, 1575−1589.
25. Armstrong, N., Sun, Y., Chen, G.-Q., and Gouaux, J. E. (1998) *Nature 395*, 913−917.
26. Abele, R., Lampinen, M., Keinänen, K., and Madden, D. R. (1998) *J. Biol. Chem. 273*, 25132−25138.
27. Bradford, M. M. (1976) *Anal. Biochem. 72*, 248−254.
28. Koch, M. H. J., and Bordas, J. (1983) *Nucl. Instrum. Methods 208*, 461−469.
29. Gabriel, A., and Dauvergne, F. (1982) *Nucl. Instrum. Methods 201*, 223.
30. Svergun, D. I. (1993) *J. Appl. Crystallogr. 26*, 258−267.

31. Svergun, D. I., Semenyuk, A. V., and Feigin, L. A. (1988) *Acta Crystallogr. A44*, 244−250.
32. Svergun, D. I. (1992) *J. Appl. Crystallogr. 25*, 495−503.
33. Svergun, D. I., Volkov, V. V., Kozin, M. B., Stuhrmann, H. B., Barberato, C., and Koch, M. H. J. (1997) *J. Appl. Crystallogr. 30*, 798−802.
34. Svergun, D. I., Volkov, V. V., Kozin, M. B., and Stuhrmann, H. B. (1996) *Acta Crystallogr. A52*, 419−426.
35. Svergun, D. I., Barberato, C., and Koch, M. H. J. (1995) *J. Appl. Crystallogr. 28*, 768−773.
36. Svergun, D. I., Volkov, V. V., and Kozin, M. B. (1997) *J. Appl. Crystallogr. 30*, 811−815.
37. Svergun, D. I., Konrad, S., Huss, M., Koch, M. H. J., Wieczorek, H., Altendorf, K., Volkov, V. V., and Grüber, G. (1998) *Biochemistry 37*, 17659−17663.
38. Ames, G. F. L. (1986) *Annu. Rev. Biochem. 55*, 397−425.
39. Abele, R. (1998), Ph.D. thesis, Ruprecht-Karls-Universität, Naturwissenschaftlich-Mathematische Gesamtfakultät, Heidelberg, Germany, pp 59−63.
40. Walmsley, A. R., Shaw, J. G., and Kelly, D. J. (1992) *J. Biol. Chem. 267*, 8064−8072.
41. Flocco, M. M., and Mowbray, S. L. (1994) *J. Biol. Chem. 269*, 8931−8936.
42. Vermersch, P. S., Tesmer, J. J. G., Lemon, D. D., and Quiocho, F. A. (1990) *J. Biol. Chem. 265*, 16592−16603.
43. Weiner, J. H., and Heppel, L. A. (1971) *J. Biol. Chem. 246*, 6933−6941.
44. Miller, D. M. I., Olson, J. S., Pflugrath, J. W., and Quiocho, F. A. (1983) *J. Biol. Chem. 258*, 13665−13672.
45. Lewis, M., Chang, G., Horton, N. C., Kercher, M. A., Pace, H. C., Schumacher, M. A., Brennan, R. G., and Lu, P. (1996) *Science 271*, 1247−1254.
46. Sauer, R. T. (1996) *Structure 4*, 219−222.
47. Sullivan, J. M., Traynelis, S. F., Chen, H. S., Escobar, W., Heinemann, S. F., and Lipton, S. A. (1994) *Neuron 13*, 929−936.
48. Wo, Z. G., and Oswald, R. E. (1996) *Mol. Pharmacol. 50*, 770−780.
49. Saper, M. A., and Quiocho, F. A. (1983) *J. Biol. Chem. 258*, 11057−11062.
50. Lampinen, M., Pentikäinen, O., Johnson, M. S., and Keinänen, K. (1998) *EMBO J. 17*, 4704−4711.
51. Chen, G. Q., Sun, Y., Jin, R., and Gouaux, E. (1998) *Protein Sci. 7*, 2623−2630.
52. Krupp, J. J., Vissel, B., Heinemann, S. F., and Westbrook, G. L. (1998) *Neuron 20*, 317−327.
53. Villarroel, A., Regalado, M. P., and Lerma, J. (1998) *Neuron 20*, 329−339.
54. Kabsch, W. (1976) *Acta Crystallogr. A32*, 922−923.

BI982928Y